The Astrophysical Journal, 666: L133–L136, 2007 September 10
© 2007. The American Astronomical Society. All rights reserved. Printed in U.S.A.

FLUX TUBES AS THE ORIGIN OF NET CIRCULAR POLARIZATION IN SUNSPOT PENUMBRAE

J. M. Borrero
High Altitude Observatory (NCAR), Boulder, CO 80301; borrero@ucar.edu
L. R. Bellot Rubio
Instituto de Astrofísica de Andalucía (CSIC), 18080 Granada, Spain; lbellot@iaa.es
and
D. A. N. Müller
European Space Agency c/o NASA Goddard Space Flight Center, Greenbelt, MD 20771; dmueller@esa.nascom.nasa.gov
Received 2007 May 14; accepted 2007 July 26; published 2007 August 16

ABSTRACT

We employ a three-dimensional magnetohydrostatic model of a horizontal flux tube, embedded in a magnetic surrounding atmosphere, to successfully reproduce the azimuthal and center-to-limb variations of the net circular polarization observed in sunspot penumbrae. This success is partly due to the realistic modeling of the interaction between the flux tube and the surrounding magnetic field.

Subject headings: Sun: magnetic fields — sunspots — techniques: polarimetric

1. INTRODUCTION

A possible scenario that explains the magnetic field configuration of the sunspot penumbra is the so-called uncombed penumbral model (Solanki & Montavon 1993). In this model, a horizontal flux tube that harbors the Evershed flow is embedded in a more vertical magnetic field. A similar configuration has been obtained by Heinemann et al. (2007), who carried out three-dimensional MHD simulations of the penumbra and found that penumbral filaments are produced by bubbles of weak and horizontal magnetic field fully embedded in a stronger and more vertical one. They also find field free gaps connected to the deeper convection zone, which appear as bright regions in the emergent intensity.

One of the most critical observations that any penumbral model must reproduce is the net circular polarization (NCP; Sánchez Almeida & Lites 1992). Different realizations of the uncombed penumbra have successfully explained these observations (Solanki & Montavon 1993; Martínez Pillet 2000; Schlichenmaier et al. 2002; Müller et al. 2002, 2006). However, Spruit & Scharmer (2006) have pointed out that the models of the uncombed penumbra published so far do not consider the effects of the external field wrapping around the flux tube. The goal of this work is to remove this point of inconsistency. As it is shown, an uncombed model that consistently considers the perturbation in the external field introduced by a cylindrical flux tube is also able to explain the NCP observed in the sunspot penumbra with surprising accuracy.

2. FLUX TUBE MODEL AND REFERENCE FRAME

Our embedded flux tube model is adopted from Borrero (2007). This model considers a cylindrical flux tube that carries the Evershed flow. The flux tube is located perpendicularly to the vertical z-axis and is embedded in an inclined potential magnetic field.

This model prescribes the magnetic field configuration in the local reference frame (LRF), $\mathcal{S} = \{e_x, e_y, e_z\}$ (see Fig. 1), the flux tube's axis being oriented along e_x. Analytical expressions for $B_x(y, z)$, $B_y(y, z)$, and $B_z(y, z)$ are taken from equations (33) and (34) in Borrero (2007). These equations take into account how the external field bends and surrounds the flux tube. Although the model is three-dimensional, variations along the x-axis are neglected. The model is described by six parameters: B_0 and γ_0 (strength and inclination of the external magnetic field far away from the flux tube), R and z_0 (radius and central position of the flux tube), and finally B_{xt0} and v_{xt0} (component of the flux tube magnetic field along the flux tube's axis and magnitude of the Evershed flow). Figure 1 (*top*) illustrates the magnetic field lines in the plane perpendicular to the tube's axis.

The velocity and magnetic field vectors enter the static momentum equation. This yields the density $\rho(y, z)$ and gas pressure $P_g(y, z)$ that ensure force balance (see Borrero 2007 for details). Once gas pressure and density are known, the temperature $T(y, z)$ is evaluated through the equation of state for ideal gases. A varying molecular weight is used to account for the partial ionization of the different atomic species.

Once all the relevant quantities are known in the LRF, $\mathcal{S}$, we project the magnetic field and velocity vectors on the observer's reference frame, $\mathcal{S}''$. This is accomplished by a rotation of angle Ψ along the vertical z-axis. This rotation ensures that the resulting x'-axis meets the line of symmetry of the sunspot. A second rotation of angle Θ along e_y' is finally needed to direct the resulting z'' along the observer's line of sight. Mathematically,

$$\mathcal{S}'' = \{e_x'', e_y'', e_z''\} = \mathcal{R}_{y'}(\Theta) \times \mathcal{R}_z(\Psi) \times \mathcal{S}, \qquad (1)$$

where $\mathcal{R}_{y'}(\Theta)$ and $\mathcal{R}_z(\Psi)$ are the corresponding rotation matrices. In this manner, we can locate the flux tube at any azimuthal position Ψ within the sunspot and place the sunspot at any heliocentric angle, Θ, on the solar disk. Thus, we can determine the line-of-sight velocity $v_{\rm los} = v_z''$, magnetic field strength B (calculated in any reference frame), inclination of the magnetic field with respect to the line of sight $\gamma = \cos^{-1}(B_z''/B)$, and the angle of the magnetic field vector in the plane perpendicular to the line of sight $\phi = \tan^{-1}(B_x''/B_y'')$. An example of $\gamma(y, z)$ is presented in Figure 1 (*bottom*).

Finally, our physical parameters are expressed as a function of (y, z), but for our radiative transfer calculations we need to know them along the line of sight. To this end, we project the observer's line of sight onto the y-z plane: $\mathcal{U} =$

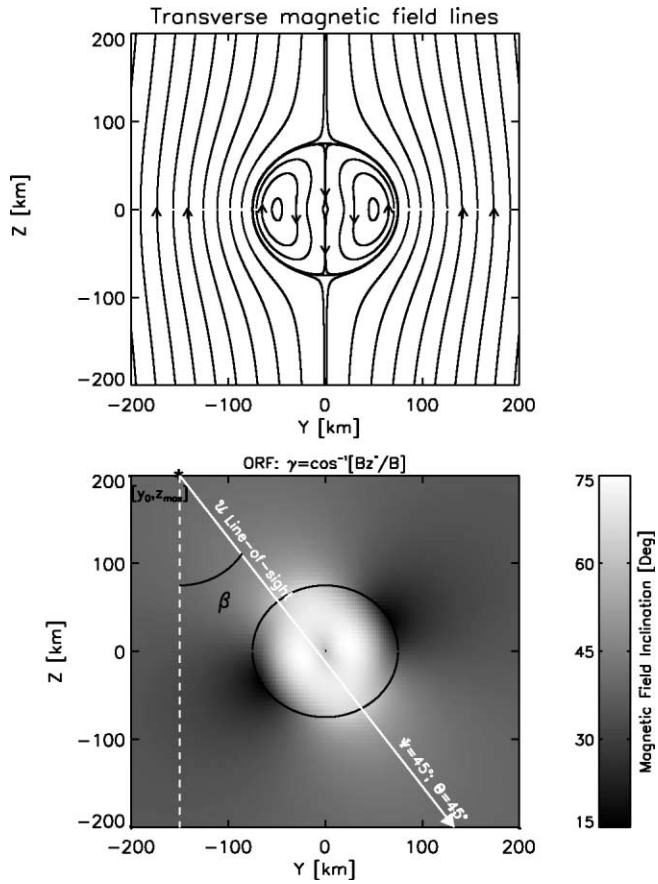

FIG. 1.—*Top*: Magnetic field lines transversal to the flux tube's axis. Note that inside the flux tube the magnetic field is mostly aligned on its axis, and therefore it is not shown here. *Bottom*: Inclination of the magnetic field in the observer's reference frame (i.e., inclination with respect to the line of sight). The white arrow represents a possible line of sight of an observer at $\Theta = 45°$ looking at a penumbral flux tube located at $\Psi = 45°$ with respect to the line of symmetry in the center side. In this example, the intersection of the ray-path with the uppermost point in the *y*-*z* plane occurs at $(y_0, z_{max}) = (-150, 200)$ km. This point is indicated by a black asterisk. The angle between the vertical *z*-axis (*white dashed line*) and the projected line of sight is $\beta \simeq 35°$. Other ray-paths would be parallel to the one drawn but intersect at different y_0.

$\sin\Psi \sin\Theta e_y - \cos\Theta e_z$. With this vector, we can construct the parametric equation of the line of sight in the *y*-*z* plane:

$$(y, z) = (y_0, z_{max}) + \lambda(\sin\Psi \sin\Theta, \ -\cos\Theta), \qquad (2)$$

where (y_0, z_{max}) is the uppermost intersection point of the ray-path with the *y*-*z* plane. The slope-intercept form of the line of sight is

$$y = y_0 + (z_{max} - z)\tan\Theta \sin\Psi. \qquad (3)$$

Note that, either at disk center ($\Theta = 0$) or along the line of symmetry of the sunspot ($\Psi = 0, \pi/2$), the ray-paths are given by $y = y_0$. At any other position, the ray-paths enter the *y*-*z* plane, forming an angle $\beta = \tan^{-1}(\tan\Theta \sin\Psi)$ with the vertical direction. As expected, $\beta = \pm\Theta$ perpendicularly to the line of symmetry ($\Psi = \pi/2, 3\pi/2$). An example of the projection of the line of sight onto the *y*-*z* plane is presented in Figure 1.

After these geometrical considerations, we are now ready to solve the radiative transfer equation and obtain theoretical Stokes profiles from our embedded flux tube model. We have

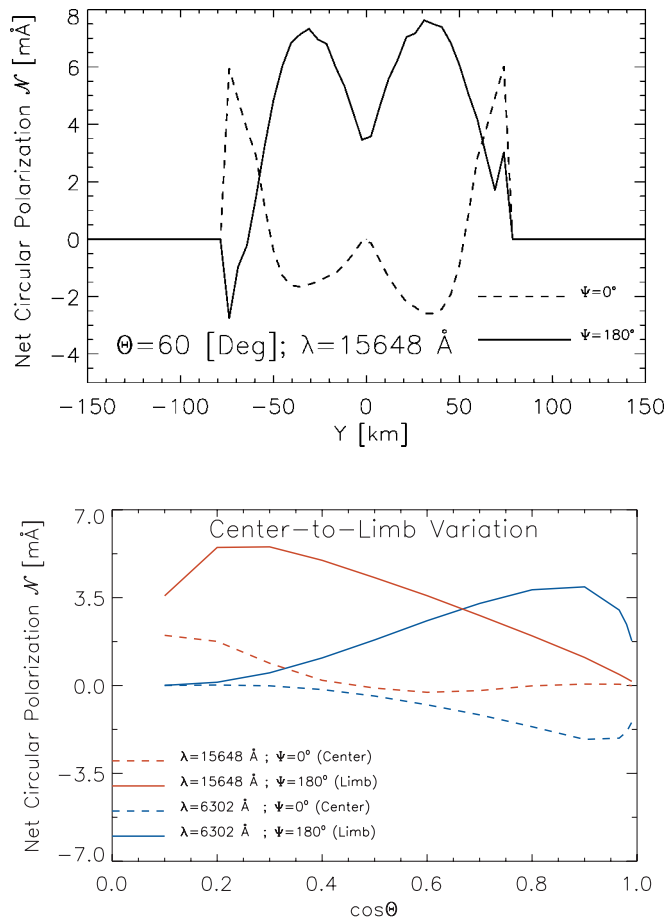

FIG. 2.—*Top*: Net circular polarization produced by each ray-path piercing the flux tube at different *y* positions. The flux tube is located at the line of symmetry on the center side (*dashed line*, $\Psi = 0$) and on the limb side (*solid line*; $\Psi = \pi$). *Bottom*: Variation of the total NCP (integral over *y* in the top panel) as a function of the heliocentric position of the sunspot: center-to-limb variation.

employed three different numerical codes—SIR (Ruiz Cobo & del Toro Iniesta 1992), DIAMAG (Grossmann-Doerth 1994), and SPINOR (Frutiger 2000)—and verified that the results are consistent among them. We first calculate the emerging polarization profiles for 128 rays that enter into the *y*-*z* plane with different y_0 (see Fig. 1). We then compute the NCP as the wavelength integral of Stokes *V*. The total NCP is obtained as sum of the NCP produced by each individual ray-path (see example in Fig. 2, *top*).

3. OBSERVATIONS

Five sunspots at five different positions on the solar disk were observed using the Tenerife Infrared Polarimeter (TIP; Martínez Pillet et al. 1999) at the Vacuum Tower Telescope (Izaña Observatory, Spain) and the Advanced Stokes Polarimeter (ASP; Elmore et al. 1992) at the Dunn Solar Telescope (Sacramento Peak, US) (see Table 1). The full Stokes vector of Fe I λ15648.5 (TIP) and Fe I λ6302.5 (ASP) were recorded. For each sunspot, radially averaged azimuthal variations of the NCP, $\mathcal{N}(\Psi)$, are computed. Here Ψ runs counterclockwise, with $\Psi = 0$ referring to the line of symmetry on the center side of the penumbra. The determination of the position of the line of symmetry from the observations is a difficult task and can only be done to an accuracy of about $\pm 10°$.

TABLE 1
SUMMARY OF OBSERVED SUNSPOTS

Active Region	Date	Θ (deg)	Fe I Line (Å)	Instrument	References
10425	2003 Aug 9	27	15648	TIP	1
8545	1999 May 21	38	6302	ASP	2
8704	1999 Sep 20	40	15648	TIP	3
10425	2003 Aug 3	50	15648	TIP	1
8706	1999 Sep 21	60	15648	TIP	4

REFERENCES.—(1) Beck 2006; (2) Borrero et al. 2006; (3) Bellot Rubio et al. 2004; (4) Borrero et al. 2005.

4. OBSERVED VERSUS THEORETICAL NCP

4.1. *Center-to-Limb Variation*

We have computed the NCP that emerges from our flux tube model for different heliocentric angles Θ. This is the so-called center-to-limb variation of the NCP. We have repeated this calculation for flux tubes located at the line of symmetry of the sunspot, on the center side ($\Psi = 0$), and on the limb side ($\Psi = \pi$). The NCP was evaluated for the same spectral lines of our observations (§ 3). Results are presented in Figure 2 (*bottom*). The parameters used for the flux tube model are $B_0 = B_{xt0} = 1000$ G, $\gamma_0 = 60°$, $v_{xt0} = 6$ km s^{-1}, $R = 75$ km, $z_0 = 0$ km. These values are consistent with results from spectropolarimetric observations of the penumbral fine structure. In addition, we have used the hot umbral model by Collados et al. (1994) to represent the thermodynamic parameters of the atmosphere surrounding the flux tube.

Martínez Pillet (2000) has presented the observed center-to-limb variation of the NCP in Fe I λ6302.5 for a large number of sunspots. Our predictions (Fig. 2, *bottom*; *blue lines*) agree very well with his findings. Our theoretical $\mathcal{N}(\Theta)$ curve for 6302.5 Å does not cross zero at $\cos\Theta = [0.8, 1]$, however. This is due to our model simplifications: the flux tube is always perpendicular to the vertical *z*-axis, and the external atmosphere does not harbor any flows.

For the near-infrared neutral iron line at 15648.5 Å, we are not aware of any similar work to that of Martínez Pillet. However, our theoretical curve is in very good agreement with other theoretical predictions that use a simpler uncombed scenario (see Müller et al. 2002, 2006). The reason is that, along the line of symmetry ($\Psi = 0, \pi$), ray-paths are not inclined on the *y*-*z* plane regardless of the heliocentric angle (eq. [3]).

4.2. *Azimuthal Variations*

In this section, we compare the observed $\mathcal{N}(\Psi)$ for different sunspots at different heliocentric angles Θ, with the theoretical predictions from the embedded flux tube model. This is done individually for each sunspot. Theoretical curves have been obtained using the same model parameters as in § 4.1. Results are presented in Figures 3 and 4. It can be seen that our model is able to reproduce many features of the observed azimuthal variations of the NCP. This achievement is especially remarkable if we consider that all we have done is change the spectral line and heliocentric angle (model parameters were kept constant).

Particularly interesting is the fact that we can also predict the existence of secondary maxima/minima in the $\mathcal{N}(\Psi)$ curves. This is clearly the case of Fe I λ15648.5, where more simple uncombed models predict only the existence of two maxima and two minima at all heliocentric angles. The improved agreement between observations and predictions is to be ascribed to our more realistic modeling of the external magnetic field bending and wrapping around the horizontal flux tube. This is a crucial ingredient for Fe I λ15648.5, where gradients in the azimuthal angle of the magnetic field play a major role (Landolfi & Landi degl'Innocenti 1996; Müller et al. 2002).

An important detail is that, in our model, the Evershed flow is channeled along the horizontal flux tube. This means that the line-of-sight velocity, $v_{\rm los} = v_z'' = -v_{xt0}\cos\Psi\sin\Theta$, vanishes always perpendicularly to the line of symmetry ($\Psi = \pi/2$, $3\pi/2$). Thus, gradients in $v_{\rm los}$ do not exist there, yielding always zero NCP. In agreement with Müller (2001), decreasing the magnitude of the Evershed flow decreases the amount of NCP roughly linearly. In the absence of a complete parameter study, this effect alone cannot be used to rule out weaker horizontal flows, however.

Borrero (2007) expressed concerns about flux tubes with circular cross sections having very smooth variations in γ. He pointed out that those variations might be too small to generate enough NCP (Sánchez Almeida & Lites 1992). Results presented in this work prove those concerns to be unfounded.

5. CONCLUSIONS

We have employed the model of Borrero (2007) to predict the behavior of the NCP in the sunspot penumbra. This model finds the equilibrium configuration of a horizontal flux tube

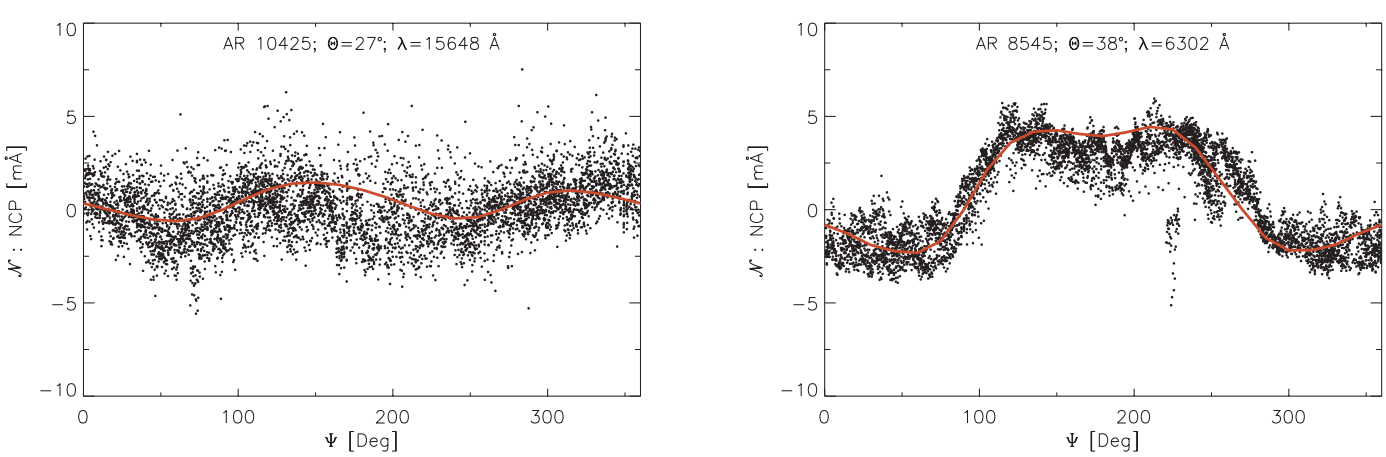

FIG. 3.—Comparison between the observed (*filled circles*) and predicted (*red solid lines*) azimuthal variations of the net circular polarization for two sunspots at heliocentric angles Θ = 27°, 38°.

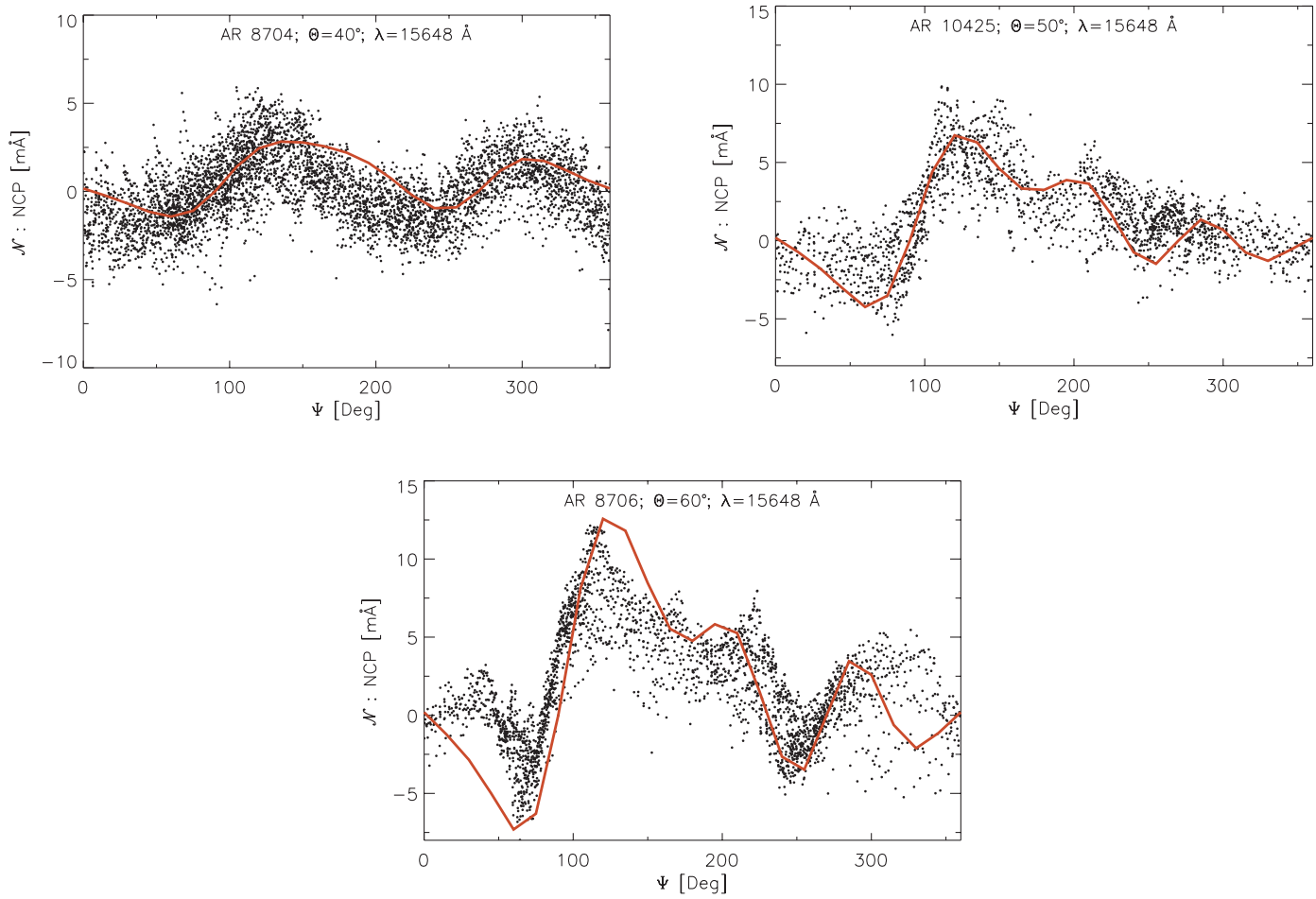

FIG. 4.—Same as Fig. 3, but for three sunspots at $\Theta = 40°, 50°, 60°$.

with circular cross section that carries the Evershed flow and is embedded in an atmosphere with a potential magnetic field pointing toward a different direction. Energy transfer is neglected, and therefore we cannot address how the penumbra is heated. This model consistently considers how the external magnetic field opens and bends in order to accommodate the horizontal flux tube. This generalizes the work of Solanki & Montavon (1993), Martínez Pillet (2000), Müller et al. (2002, 2006), and Schlichenmaier et al. (2002), by considering the three-dimensional geometry of the problem.

We have compared our predictions with the observed NCP in two neutral iron lines and in five different sunspots. The agreement between theory and observations is remarkable, improving previous determinations based on simpler realizations of the uncombed penumbral model. Other models for the penumbral fine structure (Sánchez Almeida 2005; Scharmer & Spruit 2006) should also try to explain these observations. In the future, we will attempt to reproduce also the full polarization profiles of these spectral lines (cf. Borrero et al. 2005, 2006; Bellot Rubio et al. 2004).

We wish to thank Daniel Cabrera Solana for kindly providing some of the observations used in this work.

REFERENCES

Beck, C. 2006, Ph.D. thesis, Albert-Ludwigs-University, Freiburg
Bellot Rubio, L. R., Balthasar, H., & Collados, M. 2004, A&A, 427, 319
Borrero, J. M. 2007, A&A, 471, 967
Borrero, J. M., Lagg, A., Solanki, S. K., & Collados, M. 2005, A&A, 436, 333
Borrero, J. M., Solanki, S. K., Lagg, A., Socas-Navarro, H., & Lites, B. 2006, A&A, 450, 383
Collados, M., Martínez Pillet, V., Ruiz Cobo, B., del Toro Iniesta, J. C., & Vázquez, M. 1994, A&A, 291, 622
Elmore, D. F., et al. 1992, Proc. SPIE, 1746, 22
Frutiger, C. 2000, Ph.D. thesis, Inst. Astron., ETH, Zürich
Grossmann-Doerth, U. 1994, A&A, 285, 1012
Heinemann, T., Nordlund, Å, Scharmer, G., & Spruit, H. C. 2007, ApJ, in press
Landolfi, M., & Landi degl'Innocenti, E. 1996, Sol. Phys., 164, 191
Martínez Pillet, V. 2000, A&A, 361, 734
Martínez Pillet, V., et al. 1999, Astron. Gesellschaft Abstr. Ser., 15, 5
Müller, D. A. N. 2001, M.S. thesis, Univ. Freiburg
Müller, D. A.N., Schlichenmaier, R., Fritz, G., & Beck, C. 2006, A&A, 460, 925
Müller, D. A. N., Schlichenmaier, R., Steiner, O., & Stix, M. 2002, A&A, 393, 305
Ruiz Cobo, B., & del Toro Iniesta, J. C. 1992, ApJ, 398, 375
Sánchez Almeida, J. 2005, ApJ, 622, 1292
Sánchez Almeida, J., & Lites, B. 1992, ApJ, 398, 359
Scharmer, G., & Spruit, H. 2006, A&A, 460, 605
Schlichenmaier, R., Müller, D. A. N., Steiner, O., & Stix, M. 2002, A&A, 381, L77
Solanki, S. K., & Montavon, C. A. P. 1993, A&A, 275, 283
Spruit, H. C., & Scharmer, G. B. 2006, A&A, 447, 343